Magnon-polaron anomaly in nonlocal spin transport through antiferromagnetic insulators

S. Mojtaba Tabatabaei [1], Rembert A. Duine,[2,3] and Babak Zare Rameshti[4,*]

[1]*Department of Physics, Sharif University of Technology, Tehran 14588-89694, Iran*

[2]*Institute for Theoretical Physics and Center for Extreme Matter and Emergent Phenomena, Utrecht University, Leuvenlaan 4, 3584 CE Utrecht, The Netherlands*

[3]*Department of Applied Physics, Eindhoven University of Technology, P.O. Box 513, 5600 MB Eindhoven, The Netherlands*

[4]*Department of Physics, Iran University of Science and Technology, Narmak, Tehran 16844, Iran*

(Received 28 September 2020; revised 9 May 2021; accepted 16 July 2021; published 29 July 2021)

We present a nonlocal spin transport theory for the coupled dynamics of magnetization and lattice vibrations in antiferromagnetic insulators. We find that magnon-polaron formation, i.e., coherently hybridized magnon and acoustic phonon modes, not only leads to anomalous features in the nonlocal spin current but also renormalizes the spin-flop transition field of the antiferromagnets. A length scale for the magnon-polaron formation below which the spin current is not affected by the lattice is also extracted from this nonlocal setup.

DOI: 10.1103/PhysRevB.104.014432

I. INTRODUCTION

Magnetization dynamics can be affected by lattice distortions and vice versa through magnetoelastic coupling (MEC), as demanded by reciprocity [1,2]. In the strong coupling regime, where the coupling rate exceeds both subsystem loss rates, MEC results in a hybridized state, i.e., a magnon polaron (MP) [3,4]. Anomalous features caused by MP formation manifest themselves in ferromagnetic insulators (FIs) in the spin Seebeck effect [5,6], where a thermal gradient drives a spin current, spin Peltier effect wherein spin bias generates a heat current [7], and ultrafast pump-probe spectroscopy [8,9]. A nonlocal spin transport experiment reveals that the nonlocal spin Seebeck effect can be suppressed rather than enhanced due to the MEC, above a characteristic length [10]. It has also been shown that there is a length scale for MP formation below which the lattice distortion does not affect the nonlocal spin current [11].

Antiferromagnets (AFs) have unique features over ferromagnets, including a lack of stray magnetic fields, which makes them more robust against magnetic fields [12]. They also have fast dynamics lying in the THz regime due to the exchange coupled oppositely oriented spins. The spin Seebeck effect in AFs at finite magnetic fields has been investigated experimentally [13,14], and theoretically [15–17]. The spin transport properties of AFs have also attracted much attention in recent years. It has been shown that spin transport in AFs by thermally generated magnons can only be achieved with broken sublattice symmetry which can be realized by either a finite magnetic field or normal metal contacts [18]. It has also been shown that the spin conductance diverges as one approaches the spin-flop transition while the spin Seebeck coefficient remains finite [17].

A nonlocal spin transport measurement [19] provides a unique tool to accurately determine the spin transport properties in metals [20], semiconductors [21], and insulators [19] by varying the injector-detector distance. This nonlocal measurement geometry has been utilized to investigate the spin Seebeck effect [22] as well as the temperature [23] and magnetic field [24] dependence of the magnon spin transport through FIs. Such a nonlocal measurement has been successfully implemented to observe long-distance spin transport, which can exceed tens of micrometers [25], and the spin Seebeck effect [26].

The level repulsion between magnons and *optical* phonons in AFs has been studied in Ref. [27] in a way that is reminiscent of the FIs, although the coupling of magnons to low-energy *acoustic* phonons was neglected. The MP formed by the coupling of magnons to the optical phonons, however, is not accessible within the transport measurements which are of great importance in elucidating the underlying low-energy physical phenomena. An anomaly in the spin Seebeck effect response in a uniaxial AF insulator due to the MP formation has been detected in a local configuration [28]. Applying a magnetic field near to the spin-flop transition field allows one of the magnon branches of AF to become tangential to the acoustics, giving rise to the formation of MP. Further increasing the magnetic field causes these modes to intersect at two points for which MEC turns them into hybridized MP states. We present a theory that demonstrates these MPs leave their fingerprint on nonlocal spin transport and could thus be probed in experiment. The coupling of magnons to the acoustic phonons not only leaves a resonant anomaly on the nonlocal spin current but also renormalizes the spin-flop transition field. We find that the nonlocal spin transport, depicted in Fig. 1, can probe a length scale for MP formation which cannot be extracted from a local measurement [28].

II. MAGNON POLARONS

We develop an effective long-wavelength theory for the coupled dynamics of magnetization and lattice displacement, which is applicable to a wide class of exchange coupled

*bzarer@iust.ac.ir

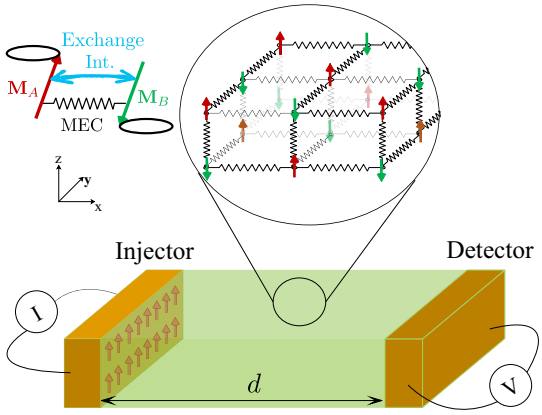

FIG. 1. Nonlocal spin transport setup: A nonequilibrium spin density accumulated in the left metallic lead by the spin Hall effect biases magnons that diffuse through the antiferromagnetic insulator, and are affected by lattice vibrations. The spin current pumped into the right metallic lead induces a nonequilibrium spin accumulation which can be detected electrically by the inverse spin Hall effect. A magnetic field H is applied to the AF in the $\mathbf{z}$ direction, and the injector-detector separation distance is denoted by d. The dynamics of two oppositely oriented sublattice magnetic moments $\mathbf{M}_A$ and $\mathbf{M}_B$, precessing around the magnetic field, are coupled through the exchange interaction and MEC.

bipartite AFs. The total free energy of the AF is $\mathcal{U} = \mathcal{U}_{\rm mag} + \mathcal{U}_{\rm el} + \mathcal{U}_{\rm mec}$, where $\mathcal{U}_{\rm mag}$ is the magnetic, $\mathcal{U}_{\rm el}$ is the elastic, and $\mathcal{U}_{\rm mec}$ is the magnetoelastic part of the AF free energy. It is convenient to describe the magnetic state of AF in a continuum representation (long-wavelength limit) using the two vectors $\mathbf{M}(\mathbf{r},t) = [\mathbf{M}_A(\mathbf{r},t) + \mathbf{M}_B(\mathbf{r},t)]/2$ and $\mathbf{l}(\mathbf{r},t) = [\mathbf{M}_A(\mathbf{r},t) - \mathbf{M}_B(\mathbf{r},t)]/2$, where $\mathbf{M}_A/\mathbf{M}_B$ represents the magnetic moment of the respective sublattice A/B at the point $(\mathbf{r},t)$. The magnetic free energy is given by

$$\mathcal{U}_{\rm mag} = s\int d\mathbf{r}\Big(\frac{a}{2}\mathbf{m}^2 + \frac{A}{2}[\nabla\mathbf{n}]^2 - \mathbf{H}\cdot\mathbf{m} - \frac{K}{2}n_z^2\Big), \quad (1)$$

where $\mathbf{n} = \mathbf{l}/|\mathbf{l}|$ is the Néel order parameter and $\mathbf{m} = \mathbf{M}/|\mathbf{M}|$ which satisfy $\mathbf{m}\cdot\mathbf{n} = 0$ well below the Néel temperature. Moreover, $s = s_A + s_B$ where $s_{A/B} = \gamma^{-1}M_{0A/B}$ is the saturation spin density of the A/B sublattice, a and A are the inter- and intrasublattice exchange constants, $\mathbf{H}$ is the external magnetic field, and K denotes the uniaxial anisotropy both taken in the $\mathbf{z}$ direction. The two sublattices can be transformed into each other by a symmetry transformation of the crystal such that the dynamic equations of $\mathbf{m}$ and $\mathbf{n}$ are invariant under an interchange of the two sublattices. The gap for one of the magnonic modes closes at the critical field, $H_c = \sqrt{K(K+a)}$, which determines the spin-flop transition point. The elastic free energy of the bipartite AF lattice is described by

$$\mathcal{U}_{\rm el} = \frac{1}{2}\sum_\chi \rho_\chi \dot{\mathbf{R}}_\chi\cdot\dot{\mathbf{R}}_\chi + \frac{1}{2}\Bigg[\sum_\chi\sum_{i=x,y,z}\sqrt{\lambda_\chi}S_{\chi,ii}\Bigg]^2 + \sum_\chi\sum_{ij=x,y,z}(\sqrt{\mu_\chi}S_{\chi,ij})^2 + \frac{1}{2}a^*(\mathbf{R}_B - \mathbf{R}_A)^2, \quad (2)$$

where $\mathbf{R}$ is the displacement vector from the equilibrium position, ρ_χ is the density of each sublattice $\chi = A/B$, a^* is the nearest-neighbor force constant, λ_χ and μ_χ are elastic constants for the respective sublattices, and $S_{\chi,ij} = \frac{1}{2}(\partial R_{\chi,i}/\partial x_j + \partial R_{\chi,j}/\partial x_i)$ is the strain tensor. The rotational deformations are ignored. In the long-wavelength limit, the magnetoelastic free energy of the AF is given by [27]

$$\mathcal{U}_{\rm mec} = 2s\sum_{i\geqslant j}B_{ij}\int dV n_i n_j S_{ij}, \quad (3)$$

where $B_{ij} = B_\parallel\delta_{ij} + B_\perp(1-\delta_{ij})$, with $B_\parallel$ ($B_\perp$) being the diagonal (off-diagonal) magnetoelastic constant. In materials with at least two sublattices, additional terms due to the internal spin structure might also be possible [27].

The coupled magnetization and lattice displacement dynamics can be obtained by minimizing the action as

$$\dot{\mathbf{n}} = -\mathbf{m}\times(\mathbf{H}_{{\rm eff},n} - \alpha\dot{\mathbf{n}}) - \mathbf{n}\times(\mathbf{H}_{{\rm eff},m} - \alpha\dot{\mathbf{m}}), \quad (4a)$$

$$\dot{\mathbf{m}} = -\mathbf{m}\times(\mathbf{H}_{{\rm eff},m} - \alpha\dot{\mathbf{m}}) - \mathbf{n}\times(\mathbf{H}_{{\rm eff},n} - \alpha\dot{\mathbf{n}}), \quad (4b)$$

$$\ddot{\mathbf{R}}_\chi = -\frac{1}{\rho_\chi}\frac{\partial\mathcal{U}}{\partial\mathbf{R}_\chi} + \frac{1}{\rho_\chi}\sum_i\frac{\partial}{\partial x_i}\frac{\partial\mathcal{U}}{\partial\frac{\partial\mathbf{R}_\chi}{\partial x_i}} - \frac{2}{\tau_p}\dot{\mathbf{R}}_\chi, \quad (4c)$$

where $\mathbf{H}_{{\rm eff},m} = -s^{-1}\delta\mathcal{U}/\delta\mathbf{m}$ and $\mathbf{H}_{{\rm eff},n} = -s^{-1}\delta\mathcal{U}/\delta\mathbf{n}$ are effective magnetic fields for $\mathbf{m}$ and $\mathbf{n}$, and α denotes the Gilbert damping of the magnetization in the bulk. A choice is made to include only one damping parameter, whereas in principle $\mathbf{n}$ and $\mathbf{m}$ may damp differently. Moreover, the relaxation time τ_p is a phenomenological damping term for the bulk lattice vibrations which is also chosen to be the same for both sublattices.

Without MEC, the ground state, which is an antiferromagnetic phase with $\mathbf{n} = \pm\mathbf{z}$ and $\mathbf{m} = \mathbf{0}$, is stable for $H \leqslant H_c$. By passing through the critical field, the system undergoes a phase transition to the spin-flopped phase where the two spins aligned nearly perpendicular to the magnetic field. To find the ground state of the coupled magnetization-elastic system we need to minimize the total free energy with respect to $\mathbf{n}$ and $\mathbf{R}$, considering that $|\mathbf{n}|^2 = 1$ and that the exchange terms disappear in the uniform state. The ground state is the antiferromagnetic phase which is stable for $H \leqslant H_c^{\rm MEC}$, where the MEC critical field is given by [32]

$$H_c^{\rm MEC} = H_c\sqrt{1 - \frac{sB_\perp^2}{K\rho\sum_{ij=A,B}c_{ij,t}^2}}, \quad (5)$$

with $c_{ij,t}$ being the transverse sound velocity of the AF and $\rho = \rho_A + \rho_B$.

In Fig. 2(a), the phonon and the magnon dispersion for the AF, including two magnon modes and an acoustic phonon branch, are shown. The finite magnetic field breaks the degeneracy between magnon modes. While increasing the magnetic field pushes the magnon and phonon modes away from each other in FIs, in contrast, here it brings the lower magnon mode into close vicinity of the acoustic branch so that they become tangential to each other at the touching magnetic field $H_{\rm T}$, shown in Fig. 2(b). Further increasing the magnetic field leads to an intersection of magnon and acoustic phonon modes. The MEC turns this intersection into hybridized magnon-

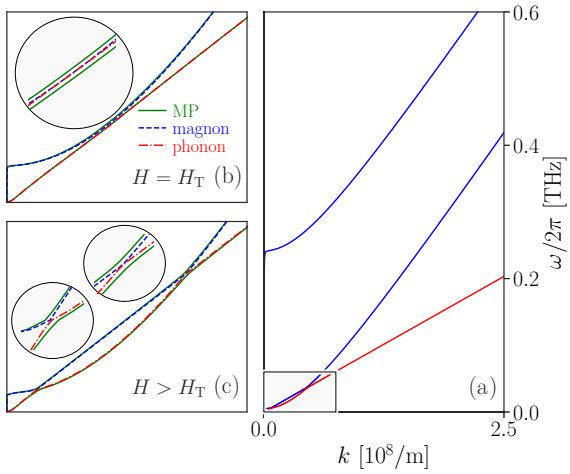

FIG. 2. (a) The antiferromagnetic insulator dispersion showing two magnon branches (blue) and an acoustic phonon branch (red). (b) At a high magnetic field $H = H_T \sim 0.93H_c$, the lower magnonic branch, the ferromagneticlike mode, touches the acoustic phonon branch. (c) By further increasing the magnetic field $H > H_T$, the lower magnonic and the acoustic phonon modes intersect at two points where the level repulsion indicates the formation of hybridized magnon-polaron states. Here, we adopt parameter values pertaining to Cr_2O_3 [29–31].

polaron states which appear as a level repulsion shown in Fig. 2(c).

III. NONLOCAL SPIN TRANSPORT

We consider a nonlocal spin transport setup in which an AF is coupled to two metallic reservoirs which serve as injector and detector (see Fig. 1). A nonequilibrium spin accumulation (spin bias) $\boldsymbol{\mu} = \mu\hat{\mathbf{z}}$ which is maintained in the injector by the spin Hall effect injects magnons into the AF. The magnons diffuse through the AF to the detector and convert to a spin accumulation at the AF|detector interface which subsequently produces a transverse charge voltage due to the inverse spin Hall effect.

Spin current through the AF bulk can be mediated by the coherent dynamics of a Néel vector coupled to the lattice displacement and by thermally generated incoherent magnons/phonons. At finite temperature, both spin and lattice fluctuations exert additional stochastic torques and forces on coupled magnetization-lattice dynamics and hence for a rigorous treatment of spin transport in such structures, both coherent and incoherent dynamics must be taken into account. The dynamics of small amplitude excitations of the coupled magnetization-lattice system ψ is governed by the linearized equations of motion in the bulk as

$$\mathscr{L}_{\rm B}\psi(x, \mathbf{q}, \omega) = -\mathfrak{h}_{\rm B}, \tag{6}$$

where $\mathbf{q}$ is the wave vector in the yz plane and $\mathscr{L}_{\rm B}$ is the bulk differential operator [32]. Here, $\mathfrak{h}_{\rm B}$ is the vector of stochastic forces arising from both magnon and phonon fluctuations which drives ψ and is related to the Gilbert damping α and phonon relaxation time τ_p by the fluctuation dissipation theorem,

$$\langle \mathfrak{h}_i(x, \mathbf{q}, \omega)\mathfrak{h}_j(x', \mathbf{q}', \omega')\rangle = (2\pi)^3\delta_{ij}\eta_i\hbar\omega\frac{\delta(x-x')\delta(\mathbf{q}-\mathbf{q}')\delta(\omega-\omega')}{\tanh\left[\hbar\omega/2k_BT_i\right]}, \tag{7}$$

where η_i denotes the dissipation along with magnetization, $\eta_{i=\delta n_x,\delta n_y} = s\alpha[1 + (H_0^2 - \omega^2)/(K + a)^2]/2$, and lattice dynamics, $\eta_{i=\rm phon} \sim \tau_p$, and k_BT_i is the local thermal energy associated with the respective subsystem. The effects of spin bias and spin/phonon noise due to the finite temperature at the metallic reservoirs are included in the AF dynamics via boundary conditions. Taking into account both deterministic and stochastic torques and forces at the AF| metal interfaces, the boundary conditions read as

$$\begin{aligned}\mathscr{L}_{\rm L}\psi(0, \mathbf{q}, \omega) &= -\mathfrak{h}_{\rm L},\\ \mathscr{L}_{\rm R}\psi(d, \mathbf{q}, \omega) &= -\mathfrak{h}_{\rm R},\end{aligned} \tag{8}$$

in which $\mathscr{L}_{\rm L(R)}$ is the boundary operator for the left (right) interface [32] and d is the injector-detector separation distance. The lattice dissipation and spin current noise result in the spin and phonon fluctuations in the left (right) normal metal $\mathfrak{h}_{\rm L(R)}$, which relates to damping coefficients η_i' according to the fluctuation-dissipation theorems

$$\langle \mathfrak{h}_{l,i}(\mathbf{q}, \omega)\mathfrak{h}_{l',j}(\mathbf{q}', \omega')\rangle = (2\pi)^3\delta_{ll'}\delta_{ij}\eta_i'(\hbar\omega - \mu_{l,i})\frac{\delta(\mathbf{q}-\mathbf{q}')\delta(\omega-\omega')}{\tanh\left[(\hbar\omega - \mu_{l,i})/2k_BT_{l,i}\right]}, \tag{9}$$

where $l, l' = {\rm L}, {\rm R}$, and η_i', giving the interfacial phonon fluctuations at the interfaces, $\eta_{i=\rm phon}' \sim \tau_p$, and the dissipation due to the spin pumping, $\eta_i' = sd\alpha'[1 + (H_0^2 - \omega^2)/(K + a)^2] - \tilde{\alpha}'2H_0/(K + a)/2$ with $\alpha' = (\alpha_A' + \alpha_B')/2$ and $\tilde{\alpha}' = (\alpha_A' - \alpha_B')/2$, in which $\alpha_\chi' = \hbar g_\chi^{\uparrow\downarrow}/(4\pi sd)$, where the spin mixing conductance $g_\chi^{\uparrow\downarrow}$ parametrizes the spin injection and pumping at the AF| metal interfaces. Here, $\mu_{l,i}$ denote the phonon and spin accumulation in the reservoirs and $T_{l,i}$ is their corresponding temperature. Both the possibilities of unbroken $\alpha_A' = \alpha_B'$ and broken $\alpha_A' \neq \alpha_B'$ sublattice symmetries at the AF|metal interfaces are considered. In our setup, a nonequilibrium spin accumulation is considered in the left normal lead and $\mu_{l,i}$ is set to zero for phonons in both leads. Without a temperature gradient, the spin current thus can be driven solely by the spin bias. The metallic reservoirs act as a perfect spin sink such that any spin accumulation generated by spin pumping at the right AF| metal interface is quickly relaxed so that the backaction effect on the coupled dynamics can be ignored. Therefore a net spin current is flowing to the right interface through AF in response to the spin bias.

We consider an AF sandwiched between two normal (heavy) metals with rotational and translational symmetries in the yz plane so that the configuration essentially is a one-dimensional problem that depends solely on the x coordinate (see Fig. 1). Within the linear approximation the Dzyaloshinskii-Moriya interaction for this configuration in which the propagation is perpendicular to the magnetic field does not contribute to the equations of motion [32] and has no

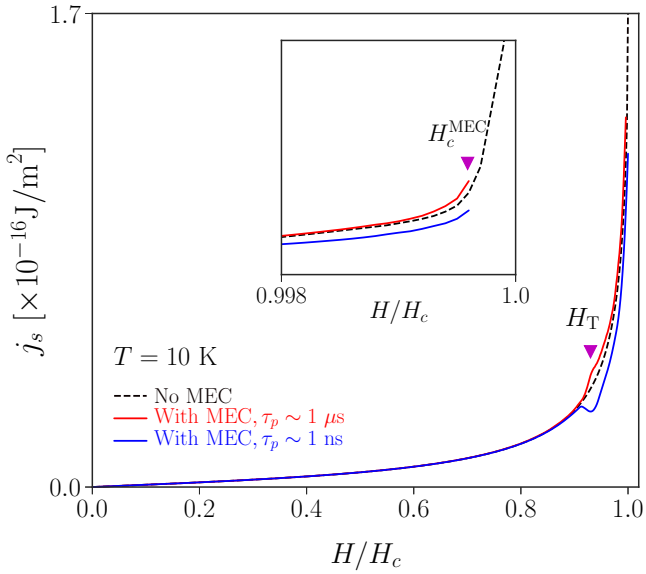

FIG. 3. Without MEC, the nonlocal spin current as a function of applied magnetic field shows an enhancement at $H = H_c$ (dashed). The MEC, however, renders the critical field H_c to a lower value H_c^{MEC} (inset). At the touching magnetic field H_{T}, the nonlocal spin current shows either a peak or a dip depending on the quality factor of the phonon transport channel. The injector-detector separation distance is fixed at $d = 5$ μm.

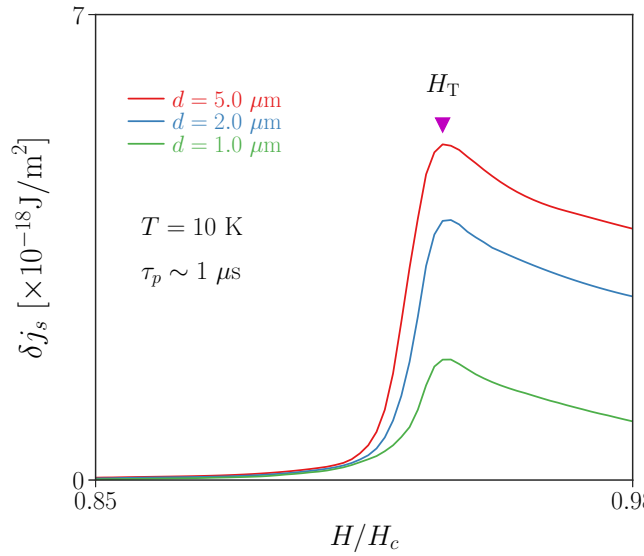

FIG. 4. The nonlocal spin current, due to the MEC, as a function of applied magnetic field for different values of injector-detector separation distance d at $T = 10$ K. The peak at the touching field decreases for the short separation distances indicating a length scale for the MP formation. The MEC strength is fixed at $B_\perp/2\pi = 0.1$ THz.

consequences for the spin transport. The thermally averaged spin current pumped into the right interface is obtained from the continuity equation as $j_s = sA\langle \mathbf{n} \times \partial_x \mathbf{n}\rangle|_d$.

The nonlocal spin current pumped to the right metal is depicted in Fig. 3 as a function of external magnetic field with MEC strength $B_\perp/2\pi = 0.1$ THz. While the sublattice symmetry breaking term at the interface, $\tilde{\alpha}'$, leads to a nonzero current even at the zero magnetic field, however, here $\tilde{\alpha}' = 0$. Without MEC, the spin current shows a strong enhancement (a divergence in the ideal case) as the magnetic field approaches the spin-flop transition point, i.e., $H = H_c$. The MEC, however, renders the magnetic field at which the nonlocal spin signal diverges to a lower magnetic field, i.e., $H = H_c^{\mathrm{MEC}}$, given by Eq. (5). This behavior can be intuitively explained by the fact that, at low temperatures, only the MP formed by the coupling of magnons with acoustic phonons gives a significant contribution to the nonlocal spin signal. By sweeping the magnetic field, the nonlocal spin current may show an anomaly as one approaches the touching field H_{T}, where the phase space formation for MP is maximized. Depending on the quality factor of the phonon transport channel, as determined by the τ_p, this anomaly manifests itself as a peak (dip) in a high-quality (deteriorated) acoustics.

The MEC contributions to the nonlocal magnon spin current $\delta j_s = j_s^{\text{With MEC}} - j_s^{\text{No MEC}}$ as a function of the applied magnetic field for varying the injector-detector distances d are depicted in Fig. 4 at $T = 10$ K. Varying the injector-detector distance in this nonlocal magnon spin transport setup allows us to extract a length scale for the MP transport. The peak indicates the touching field where the MEC contribution is maximized. By shrinking the injector-detector distances the peak decreases and finally disappears, revealing a length scale associated with the MP transport. The MP formation length scale below which the MEC does not affect the magnon spin transport is determined by dephasing of the MP and its group velocity. The length scale is thus given by $\xi_{\mathrm{MEC}} \sim \hbar v_g/\Delta_{\mathrm{MEC}}$, where v_g is the group velocity of MP and Δ_{MEC} denotes the gap between the magnons and phonons [11]. With our model parameter, $\xi_{\mathrm{MEC}} \sim 1$ μm, which is in good agreement with the numerical results. At short lengths $d < \xi_{\mathrm{MEC}}$, the lattice distortion does not influence the nonlocal spin signal and magnons need to propagate over this length scale to integrate with the acoustic transport channel.

IV. CONCLUSIONS

We studied the coupled dynamics of the magnetization and lattice vibrations in AFs. At low energies, the hybridized states between magnons and acoustic phonons can render the spin-flop transition point to a lower magnetic field. We propose the nonlocal spin transport to probe the MP formation, and have shown that MEC engenders an enhancement of the spin current. The dependence of the spin current signal on the injector-detector distance uncovers a length scale below which the MP formation cannot alter the spin current. The proposed system not only provides a deeper insight into the complete physics governing the magnon transport in AFs but also offers another platform to explore the length scale for MP formation.

ACKNOWLEDGMENTS

This research was supported by Institute for Research in Fundamental Sciences (IPM), Iran's National Elites Foundation (B.Z.R.), and Iran Science Elites Federation (ISEF)

(S.M.T. and B.Z.R.), and by the European Research Council via Consolidator Grant No. 725509 SPINBEYOND. R.A.D. is thankful for support as a member of the D-ITP consortium, a program of the Netherlands Organisation for Scientific Research (NWO) that is funded by the Dutch Ministry of Education, Culture and Science (OCW).

[1] C. Kittel, Phys. Rev. **110**, 836 (1958).
[2] E. Schlömann, J. Appl. Phys. **31**, 1647 (1960).
[3] A. Kamra, H. Keshtgar, P. Yan, and G. E. W. Bauer, Phys. Rev. B **91**, 104409 (2015).
[4] A. Rückriegel, P. Kopietz, D. A. Bozhko, A. A. Serga, and B. Hillebrands, Phys. Rev. B **89**, 184413 (2014).
[5] B. Flebus, K. Shen, T. Kikkawa, K. I. Uchida, Z. Qiu, E. Saitoh, R. A. Duine, and G. E. W. Bauer, Phys. Rev. B **95**, 144420 (2017).
[6] T. Kikkawa, K. Shen, B. Flebus, R. A. Duine, K. I. Uchida, Z. Qiu, G. E. W. Bauer, and E. Saitoh, Phys. Rev. Lett. **117**, 207203 (2016).
[7] R. Yahiro, T. Kikkawa, R. Ramos, K. Oyanagi, T. Hioki, S. Daimon, and E. Saitoh, Phys. Rev. B **101**, 024407 (2020).
[8] K. Shen and G. E. W. Bauer, Phys. Rev. Lett. **115**, 197201 (2015).
[9] N. Ogawa, W. Koshibae, A. J. Beekman, N. Nagaosa, M. Kubota, M. Kawasaki, and Y. Tokura, Proc. Natl. Acad. Sci. U.S.A. **112**, 8977 (2015).
[10] L. J. Cornelissen, K. Oyanagi, T. Kikkawa, Z. Qiu, T. Kuschel, G. E. W. Bauer, B. J. van Wees, and E. Saitoh, Phys. Rev. B **96**, 104441 (2017).
[11] B. Zare Rameshti and R. A. Duine, Phys. Rev. B **99**, 060402(R) (2019).
[12] V. Baltz, A. Manchon, M. Tsoi, T. Moriyama, T. Ono, and Y. Tserkovnyak, Rev. Mod. Phys. **90**, 015005 (2018).
[13] S. M. Wu, W. Zhang, A. KC, P. Borisov, J. E. Pearson, J. S. Jiang, D. Lederman, A. Hoffmann, and A. Bhattacharya, Phys. Rev. Lett. **116**, 097204 (2016).
[14] S. Seki, T. Ideue, M. Kubota, Y. Kozuka, R. Takagi, M. Nakamura, Y. Kaneko, M. Kawasaki, and Y. Tokura, Phys. Rev. Lett. **115**, 266601 (2015).
[15] Y. Ohnuma, H. Adachi, E. Saitoh, and S. Maekawa, Phys. Rev. B **87**, 014423 (2013).
[16] S. M. Rezende, R. L. Rodríguez-Suárez, and A. Azevedo, Phys. Rev. B **93**, 014425 (2016).
[17] S. A. Bender, H. Skarsvåg, A. Brataas, and R. A. Duine, Phys. Rev. Lett. **119**, 056804 (2017).
[18] R. Cheng, J. Xiao, Q. Niu, and A. Brataas, Phys. Rev. Lett. **113**, 057601 (2014).
[19] L. J. Cornelissen, J. Liu, R. A. Duine, J. B. Youssef, and B. J. van Wees, Nat. Phys. **11**, 1022 (2015).
[20] F. J. Jedema, A. T. Filip, and B. J. van Wees, Nature (London) **410**, 345 (2001).
[21] X. Lou, C. Adelmann, S. A. Crooker, E. S. Garlid, J. Zhang, K. S. M. Reddy, S. D. Flexner, C. J. Palmstrøm, and P. A. Crowell, Nat. Phys. **3**, 197 (2007).
[22] K. Ganzhorn, T. Wimmer, J. Cramer, R. Schlitz, S. Geprägs, G. Jakob, R. Gross, H. Huebl, M. Kläui, and S. T. B. Goennenwein, AIP Adv. **7**, 085102 (2017).
[23] L. J. Cornelissen, J. Shan, and B. J. van Wees, Phys. Rev. B **94**, 180402(R) (2016).
[24] L. J. Cornelissen and B. J. van Wees, Phys. Rev. B **93**, 020403(R) (2016).
[25] R. Lebrun, A. Ross, S. A. Bender, A. Qaiumzadeh, L. Baldrati, J. Cramer, A. Brataas, R. A. Duine, and M. Kläui, Nature (London) **561**, 222 (2018).
[26] G. R. Hoogeboom and B. J. van Wees, Phys. Rev. B **102**, 214415 (2020).
[27] H. T. Simensen, R. E. Troncoso, A. Kamra, and A. Brataas, Phys. Rev. B **99**, 064421 (2019).
[28] J. Li, H. T. Simensen, D. Reitz, Q. Sun, W. Yuan, C. Li, Y. Tserkovnyak, A. Brataas, and J. Shi, Phys. Rev. Lett. **125**, 217201 (2020).
[29] S. Foner, Phys. Rev. **130**, 183 (1963).
[30] L. R. Rossi and W. G. Lawrence, J. Am. Ceram. Soc. **53**, 604 (1970).
[31] K. D. Belashchenko, O. Tchernyshyov, A. A. Kovalev, and O. A. Tretiakov, Appl. Phys. Lett. **108**, 132403 (2016).
[32] See Supplemental Material at http://link.aps.org/supplemental/10.1103/PhysRevB.104.014432 for a detailed derivation of the equations of motion and boundary conditions.